Environmental Technology & Innovation 15 (2019) 100376

Contents lists available at ScienceDirect

Environmental Technology & Innovation

journal homepage: www.elsevier.com/locate/eti

Rapid absorption of ethylene oxide exhaust by catalytic hydration on acid zeolite catalysts

Bin Sun, Meijun Wen, Xiaobin Ma, Ying Zhou, Qiulian Zhu, Hanfeng Lu *

Innovation Team, Air Pollution Control, Institute of Catalytic Reaction Engineering, College of Chemical Engineering, Zhejiang University of Technology, Hangzhou 310014, China

HIGHLIGHTS

- A methodology is presented to remove EO by catalytic absorption at room temperature.
- The method is considered low-cost, energy-saving and environment-friendly proposal.
- The removal efficiency of EO can reach approximately 99% (higher than 1% H_2SO_4 (93%)).

GRAPHICAL ABSTRACT

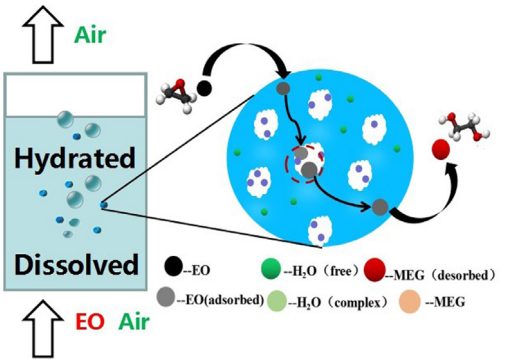

ARTICLE INFO

Article history:
Received 9 December 2018
Received in revised form 12 April 2019
Accepted 13 April 2019
Available online 18 April 2019

Keywords:
EO removal
Solid acid
Absorption
Hydration

ABSTRACT

Using a mineral acid, such as sulfuric acid, as a catalyst would cause serious environmental contamination. The use of such an acid requires subsequent distillation despite its efficiency to catalyze the absorption of ethylene oxide (EO) exhaust by water. This paper reports an energy-saving and environmentally friendly strategy to replace mineral acid with solid acid. Microporous silicon–aluminum zeolites, such as H-ZSM-5, HY, and H β, were previously shown to be strong solid acid materials. In this study, we investigate the effect of the acidity of these materials on the catalytic absorption of EO exhaust. The H-ZSM-5 with strongest Brønsted acidity exhibited the best performance. Furthermore, the intrinsic reaction kinetics indicated that the reaction conducted with and without a catalyst follows a first-order irreversible reaction model in which the reaction rate and activation energy toward the consumption of EO was greatly changed (k rate constant improved by 0.145 g^{-1} s^{-1} and Ea activation energy decreased by 13 kJ/mol).

* Correspondence to: Zhejiang University of Technology, 18# Chaowang Road, Hangzhou 310014, China.
E-mail address: luhf@zjut.edu.cn (H. Lu).

https://doi.org/10.1016/j.eti.2019.100376

1. Introduction

As a new generation of surface disinfectant, ethylene oxide (EO) is widely used in hospitals and the medical equipment industry to replace steam in the sterilization of heat-sensitive tools and equipment, such as disposable plastic syringes (McKetta and Cunningham, 1984). EO can react with carboxyl, amine, sulfhydryl, and hydroxyl groups of protein to destroy bacterial activity (Pinto, 2006). However, EO is extremely flammable and explosive because of its ultra-low boiling point. EO is also one of the major components of volatile organic compounds (Lu et al., 2013; Li et al., 2018; Kamal et al., 2016; Chen et al., 2018). The national standard for maximum EO emission is 2.5 ppm (GB/T 13098, 2006). However, in practical applications, the concentration of EO exhaust reaches several hundred thousand ppm after single sterilization. Recent efforts have focused on the treatment of EO exhaust through combustion (Yang, 1982), adsorption (Cheng, 2013), and biodegradation (Yang and Zhang, 2014) . However, these methods are usually proven unsafe, corrosive, and costly. In previous studies, absorption was found to be safe, economical, and capable of effective treatment of EO exhaust, which was accomplished through the rapid hydration of EO with H_2O.

The rate of EO hydrolysis is dependent upon the pH level of the aqueous solution. In neutral water (pH = 7), the half-life of dissolved EO was reported by Conway et al. (1983) to be approximately 10 days. Moreover, Conway et al. (1983) found that the half-life of dissolved EO rapidly decreases as the pH of the solution decreases to below 3. The mineral acid was generally used to decrease the pH of the solution such as sulfuric acid (Altiokka and Akyalcin, 2009). The hydration process went through protonation, ring opening, additive reaction, and neutralization. A large amount of waste acids had to be neutralized, and substantial aqueous salt waste could cause serious environmental contamination.

With the expansion of environmental awareness, developing new non-toxic and highly effective catalysts has become a major research topic in the area of green catalysis. The replacement of mineral acid with solid acid catalysts may provide a solution to environmental pollution problems. The use of solid acid has inherent advantages over catalysis affected by dissolved electrolytes because the former eliminates the corrosive environment and can be easily removed from the reaction mixture by decantation and filtration (Maihom et al., 2008).

The hydration of EO has been studied by many researchers to produce monoethylene glycol (MEG) in the presence of heterogeneous catalysis (Shvets et al., 2005). Acid ion-exchange resin (Lemanski and Kunin, 2000), heteropolyacids (Hal et al., 2007), sulfonated silicone gel (Wang et al., 2005), niobium oxide supported on α-alumina (Li et al., 2005, 2006), and layered niobic acid (Yang et al., 2011) have been used as solid acid catalysts. Both of the catalysts have good performance in EO hydration at 100 ° C and 1–2 Mpa (conversion rate of EO was 95% in 0.5 h).

However, for these solid acids, non-negligible deficiency is an issue because they have few acidic sites, no stable pore structure, and can easily lose acidic groups despite their high catalytic performance at high temperature and pressure. As a solid acid, zeolites are microporous aluminosilicate crystalline minerals with exchangeable cations that have important functions in the chemical and petrochemical industries (Li et al., 2016; Chen and Li, 2018). This important role is due to the unique properties of zeolite, such as high surface area, uniform porosity, high ion-exchange capacity, strong acidity, and high (hydro)thermal stability (Al-Jubouri and Holmes, 2017) (Olegario et al., 2018). The pores of zeolites, especially ZSM-5, have strong shape selectivity. In addition, EO is easily adsorbed on the active site of the zeolite due to strong polarity on the surface of the zeolite and strong polarity of EO (permittivity 14).

This study investigates the catalytic performance of zeolites compared with H_2SO_4 in the removal of EO. The catalytic activity of Hβ, HY, and H-ZSM-5 was first scanned, and then the catalytic performance of H-ZSM-5 for this hydration reaction was further examined. Results would establish the foundation of a green and environmentally friendly technology for EO treatment.

2. Experiments

2.1. Materials

The chemicals used in the present work, including ethylene oxide, ethylene glycol, molecular sieve, and deionized water, were commercially purchased and used without further purification.

2.2. Characterization

Infrared (IR) spectra of pyridine adsorption were recorded on a VERTEX 70 FTIR spectrometer with 6 cm^{-1}resolution. For the pyridine adsorption experiment, the sample disk containing catalyst was heated at 673 K and evacuated for 1 h, and then cooled to room temperature and exposed to pyridine vapor for 1 h. Thereafter, the excess pyridine was purged with N_2 for 1 h. The spectra of the adsorbed pyridine were recorded at room temperature.

The specific surface area and porosity of all the samples were calculated for the nitrogen adsorption–desorption isotherms at 77 K with a Micromeritics 3Flex Surface Characterization Analyzer.

X-ray diffraction (XRD) patterns were recorded on an X'pert PRO diffractometer (PANalytical, Netherlands) using Cu K_α radiation at a generator voltage of 40 kV and tube current of 40 mA. The samples were scanned in the 2θ range of 10°–80° with scanning speed of 0.02° s^{-1}. Diffraction peaks were compared with the standard Joint Committee on Powder Diffraction Standard (JCPDS) database reported by the International Centre for Diffraction Data.

Table 1
Surface area, pore volume and pore diameter of zeolites.

Zeolites	$S_{BET}/(m^2.g^{-1})$	$V_{pore}/(cm^3.g^{-1})$	D_{pore}/nm
Hβ-25	504	0.245	0.676
HY-5.7	570	0.282	0.669
H-ZSM-5-25	283	0.141	0.612
H-ZSM-5-38	374	0.186	0.600
H-ZSM-5-81	290	0.131	0.642
H-ZSM-5-200	363	0.168	0.614

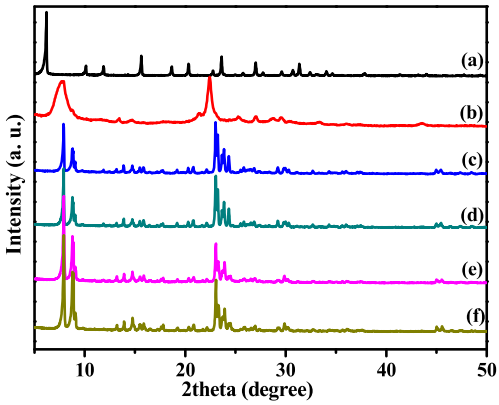

Fig. 1. XRD patterns of zeolites (a) Hβ-25, (b) HY-5.7, (c) H-ZSM-5-25, (d) H-ZSM-5-38, (e) H-ZSM-5-81, (f) H-ZSM-5-200.

2.3. Catalytic activity measurement

The absorption of ethylene oxide was conducted in a fluidized-bed U-tube (internal diameter of 25 mm and length of 300 mm) with sand core at the bottom at 303 K. For this experiment, we used 2.0 g of catalyst with a total flow rate of the feed stream at 100 mL min^{-1}, providing a space velocity of 3000 mL g^{-1} h^{-1}. The feed stream containing 10,000 ppm ethylene oxide was generated by bubbling air through a saturator containing pure ethylene oxide chilled in an ice-water isothermal bath, and then diluted with another air steam by the mass flow controller. The volume of absorbent was 50 mL. The gas stayed in the solution for 7.3 s. The concentration of ethylene oxide at the outlet of the reactor was monitored with a gas chromatograph (Agilent, G6890N) equipped with a flame ionization detector. The removal efficiency of EO was calculated using the following equation:

$$\text{EO removal efficiency} = ([EO]_{in} - [EO]_{out})/[EO]_{in} = (C_0 - C)/C_0.$$

We also performed dynamic analysis of EO. The hydration reaction was conducted in an isothermal batch autoclave reactor with different water/ethylene oxide molar ratios under continuous stirring (200 rpm) at 303, 313, and 323 K. The products were analyzed on a GC6890N gas chromatograph equipped with a column and a flame ionization detector.

3. Results and discussion

3.1. Structural and textural properties of catalysts

The textural properties of all catalysts are presented in Table 1. As the table shows, HY and Hβ have higher BET surface areas than H-ZSM-5. The BET surface areas increase with the silica–alumina ratio for H-ZSM-5 except for H-ZSM-5-38, which has the highest specific surface area among the H-ZSM-5. All zeolites have similar pore diameters and microporous channels. This characteristic is consistent with previous reports (Li et al., 2016; Chen et al., 2018).

To gain in-depth insight into the structure evolution, we measured the XRD patterns of the zeolites, as shown in Fig. 1. The XRD patterns are identical to those of faujasite (JCPDS Card No. 26-0896), β (JCPDS Card No. 47-0183), and ZSM-5, (H) (JCPDS Card No. 42-0024). The match between composite pattern and pure form zeolite indicates that the materials we used are exactly three typical zeolites.

3.2. Acidity measurements

Fig. 2 shows the IR spectra of pyridine adsorption in the range of 1700–1400 cm^{-1} on the H-ZSM-5, HY, and Hβ catalysts with Si/Al mole ratios of 25, 5.7, and 25, respectively.

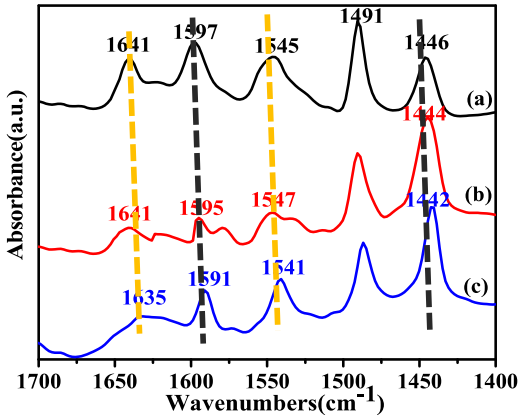

Fig. 2. IR spectra of pyridine adsorption on three Zeolites at room temperature. (a) H-ZSM-5-25, (b) Hβ-25, (c) HY-5.7.

Table 2
The acid type and number of sites for the zeolites used at room temperature and EO removal efficiency at 90 min under catalysis.

Acidic	Lewis acidic sites		Brønsted acid sites			
Zeolites	Integral area[a] [cm^{-1}]	$Number_{py}$[b] [μmol/g]	Integral area [cm^{-1}]	Number [μmol/g]	Total number [μmol/g]	X_{EO} (t = 90 min)
Hβ-25	4.04	135	1.20	53.0	188	87.0%
HY-5.7	2.86	95.3	1.05	46.3	142	68.6%
H-ZSM-5-25	2.29	76.3	2.74	121	197	98.9%
H-ZSM-5-38	5.56	185	4.09	180	365	99.1%
H-ZSM-5-81	3.87	129	/	/	129	98.6%
H-ZSM-5-200	3.64	121	/	/	121	97.5%

[a]Integration regions approximately 1525–1565 cm^{-1} and 1425–1470 cm^{-1}, respectively.
[b]Emeis' procedure was applied for calculation. py=pyridine.

The absorptions at ~1610 and ~1450 cm^{-1} were assigned to pyridine adsorbed on Lewis acid sites (LASs), and the absorption at 1550 cm^{-1} accompanied by other peaks near 1640–1620 $cm^{-1}$was assigned to pyridine adsorbed on Brønsted acid sites (BASs). The wavenumber of the strength of the band at approximately 1610 cm^{-1} provides information on the strength of the LASs, and the intensity of the band at ~1450 cm^{-1} is related to the number of LASs (Corma, 1995; Ziolek et al., 1997). For all catalysts, absorption bands at approximately 1450 and 1550 cm^{-1} were observed at room temperature, indicating that both BASs and LASs exit on the surface of the catalysts. The acid type and number of sites (Emeis, 1993) for the zeolites used at room temperature are summarized in Table 2. H-ZSM-5-25 has fewer LASs (76.3 $umol_{py}/g$) (py = pyridine) and more BASs (121 $umol_{py}/g$) than those of Hβ-25 and HY-5.7, and the highest total number of acid sites (197 $umol_{py}/g$).

Fig. 3 shows the IR spectra of pyridine adsorption in the range of 1700–1400 cm^{-1}on H-ZSM-5 for different silica–alumina ratio at 25, 38, 81, and 200. The FTIR of pyridine adsorption provided minimal quantitative information on Brønsted acidity because no adsorption band was registered at approximately 1550 and 1640 cm^{-1} for H-ZSM-5-81 and H-ZSM-5-200. Similarly, the acid type and number of sites of the zeolites used at room temperature are summarized in Table 2. The order of the total number of acid sites was H-ZSM-5-38 > H-ZSM-5-25 > H-ZSM-5-81 > H-ZSM-5-200.

3.3. Absorption properties of EO

The catalytic activities of the zeolites in EO absorption were tested under the base condition of EO inlet concentration of 10000 ppm and WHSV of 3000 mL $h^{-1}g^{-1}$at room temperature. For every experiment, the volume of absorbent was 50 mL. The results are presented in Fig. 4. Fig. 4a shows the absorption curve of EO over three kinds of zeolites, 1% H_2SO_4, and pure water. In the blank experiment (without catalysts), the removal efficiency of EO decreased rapidly (< 60% at 90 min). These results indicated that the direct hydration efficiency of EO under test conditions and in the absence of catalysis was low. By contrast, the zeolites achieved high EO removal efficiency (> 68% at 90 min). For Hβ and HY, the curves decreased slightly (the curve for HY-5.7 was steeper). Furthermore, the H-ZSM-5 zeolite had maximum absorption efficiency (> 98%) among all zeolites and the curve remained steady. Moreover, the removal efficiency was higher than that of 1% H_2SO_4(v/v) (93%).

As an acid-catalyzed reaction, the catalytic activity of a zeolite depended on its of acid, surface, and structural properties. As illustrated in Fig. 2, the IR spectra of pyridine adsorption indicate the difference in acid site density, acidity, and acid strength among the three zeolites. Table 2 shows the total number of BAS and LAS sites. H-ZSM-5-25, which

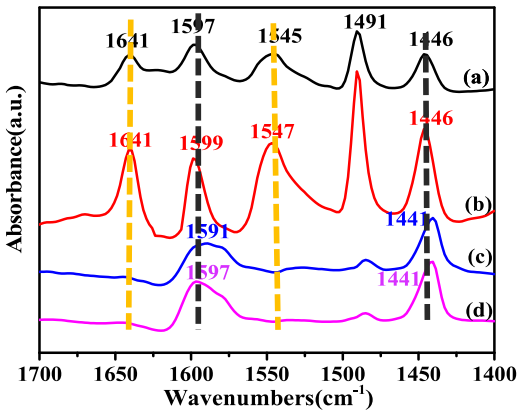

Fig. 3. IR spectra of pyridine adsorption on H-ZSM-5 catalyst for different silica-alumina at (a) 25, (b) 38, (c) 81, (d) 200, respectively.

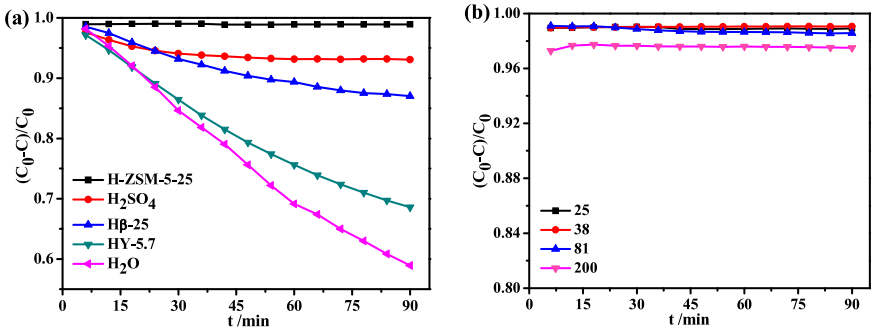

Fig. 4. (a) Absorption curves of ethylene oxide for three different zeolites. (b) Adsorption curves of ethylene oxide for H-ZSM-5 for different silica–alumina ratio at 25, 38, 81 and 200, respectively. Other conditions: ethylene oxide concentration 10000 ppm and WHSV 3000 mL h^{-1} g^{-1}; absorbent volume 50 mL; absorption temperature 30 °C.

has fewer LASs but more BASs, exhibited the best performance, which illustrated that Brønsted sites played a dominant role in the EO catalysis. The surface area, pore volume, and pore diameter of zeolites are summarized in Table 1. HY-5.7 and Hβ-25 have similar pore openings and volumes, but HY-5.7 exhibited poor performance due to low acid density and weakness.

Fig. 4b shows the absorption curve of EO on H-ZSM-5 over different silica–alumina ratios. The catalytic activity was in the order of H-ZSM-5-38 > H-ZSM-5-25 > H-ZSM-5-81 > H-ZSM-5-200. Similarly, the IR spectra of pyridine adsorption, number of BAS and LAS sites, and textural properties of catalysts are presented in Fig. 3, Table 1, and Table 2. H-ZSM-5-38, which has a large surface area (374 m^2/g) and small pore opening (0.600 nm), is excellently active because EO diffusion is wider, whereas H-ZSM-5-200, which has a surface area of 363 m^2/g, is poorly active due to low acid density. Although the total acid amounts of H-ZSM-5-81 and H-ZSM-5-200 are lower than those of HY and Hβ, they have higher activity because the Z-type pores of ZSM-5 are more favorable for shape-selective catalysis.

3.4. Effect of concentration and space velocity

In practical applications, the concentration of EO is changeable. Good catalytic activity at each concentration without dilution would be convenient. The catalytic activity of the zeolite remained stable (Fig. 5a) by increasing the EO concentration (5000–40000 ppm). This result indicated that the zeolite was capable of treating EO exhaust gas with a wide range of concentration changes. Moreover, space velocity is an important parameter in the practical application of catalysts. To achieve high EO removal efficiency, a high space velocity is required for catalysts. Thus, the catalytic behavior of the H-ZSM-5-38 zeolite in EO absorption under four different WHSV values was tested (Fig. 5b). Increasing the WHSV values has a minimal effect on the removal of EO. When the space velocity reaches 24000 mL/(g·h), the curve shows a downward trend. This result may be attributed to the shortened residence time of EO in the solution at high WHSV. Nevertheless, the result suggested that the catalyst could be used to catalyze the conversion of high EO fluxes. Thus, the zeolite has application potential in the EO treatment field.

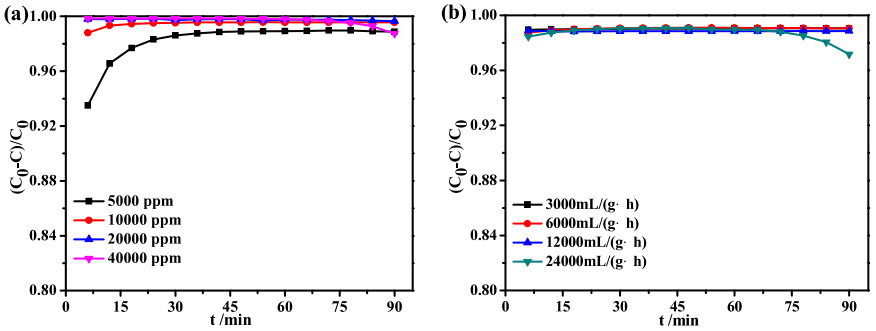

Fig. 5. Effect of Concentration and Space velocity. (a) Absorption curves of ethylene oxide over H-ZSM-5-38 catalysis under different concentration. Other conditions: ethylene oxide WHSV 3000 mL h^{-1} g^{-1}. (b) Effect of space velocity on ethylene oxide absorption over H-ZSM-5-38. Other conditions: ethylene oxide concentration of 10000 ppm. Absorbent volume 50 mL; absorption temperature 30 °C.

3.5. Kinetics of EO hydration

3.5.1. Kinetic equation

The overall reaction rate depends on the reaction of EO and water on the surface of zeolite. That is, the rate-determining step of the entire reaction is the reaction of adsorbed EO and water on the zeolite. Thus, we establish a dynamic equation based on the Hougen–Watson mechanism, which indicates reaction rate with adsorbate and vacancy concentration. The rate equation can be given by

$$r = [N_S]^2 \frac{k_s K_A K_B C_A C_B}{[1 + K_A C_A + K_B C_B + K_C C_C]^2}, \tag{3.1}$$

where A, B, and C are H_2O, EO, and MEG. Furthermore, $[N_0]$, $[N_i]$, and $[N_S]$ are the concentrations of vacant sites, active sites occupied by absorbent, and total active sites of the catalyst, respectively. $[K_A]$, $[K_B]$, and $[K_C]$ are the adsorption equilibrium constants of A, B, and C.

The amount of water was much higher than that of EO and MEG, and was adsorbed strongly on the surface of the catalyst. Thus, water concentration can be regarded as a constant and $K_A C_A \gg 1$.

$$r = [N_S]^2 \frac{k_s K_B C_B}{K_A C_A} \tag{3.2}$$

$$r = \frac{dC_{MEG}}{dt} = -\frac{dC_{EO}}{dt} = k_r C_{EO} \tag{3.3}$$

$$k_r = [N_S]^2 \frac{k_s K_B}{K_A C_A} = A \cdot e^{-\frac{E_a}{RT}}. \tag{3.4}$$

Then, Eqs. (3)–(5) was evaluated numerically to obtain the average reaction rate under prescribed conditions (Shvets et al., 2005).

$$-r_{EO,av} = \frac{\int_{C_0}^{C} -r_{EO} dC}{C - C_0}. \tag{3.5}$$

3.5.2. Experimental data and kinetic parameters

Experiments were conducted at constant catalyst addition of 10 mg and with EO concentration of 1% (v/v), while temperature varied at 303, 313, and 323 K. Also, the uncatalyzed reactions were performed with the same reaction conditions. The curve of EO concentration with time is shown in Fig. 6. The hydration reaction of ethylene oxide was found to be a first-order reaction by fitting the EO concentration. The calculated reaction rate constants are presented in Table 3, and the Arrhenius curve under catalytic and non-catalytic reactions are shown in Fig. 7b. The reaction rate was improved significantly with the addition of H-ZSM-5. The first-order reaction rate constant was 0.296 s^{-1} g^{-1} (303 K), which was double that of water (0.142 s^{-1} g^{-1}). The activation energy was reduced by 13 kJ/mol. The calculated reaction rate of the catalyzed hydration reaction at 303 K is shown in Table 4. H-ZSM-5 has better catalytic efficiency (0.0989 μmol L^{-1} s^{-1} m^{-2}) than Hβ (0.0502 μmol L^{-1} s^{-1} m^{-2}) and HY (0.0316 μmol L^{-1} s^{-1} m^{-2}).

3.5.3. Effect of diffusion

The hydration process of EO catalyzed by zeolite can be divided into the following steps: (1) EO and water diffuse to the surface of zeolite; (2) EO and water are adsorbed on the active site of zeolite; (3) the adsorbed ethylene oxide reacts with water to form adsorbed alcohol; (4) the adsorbed alcohol is desorbed from the surface of zeolite; and (5) the

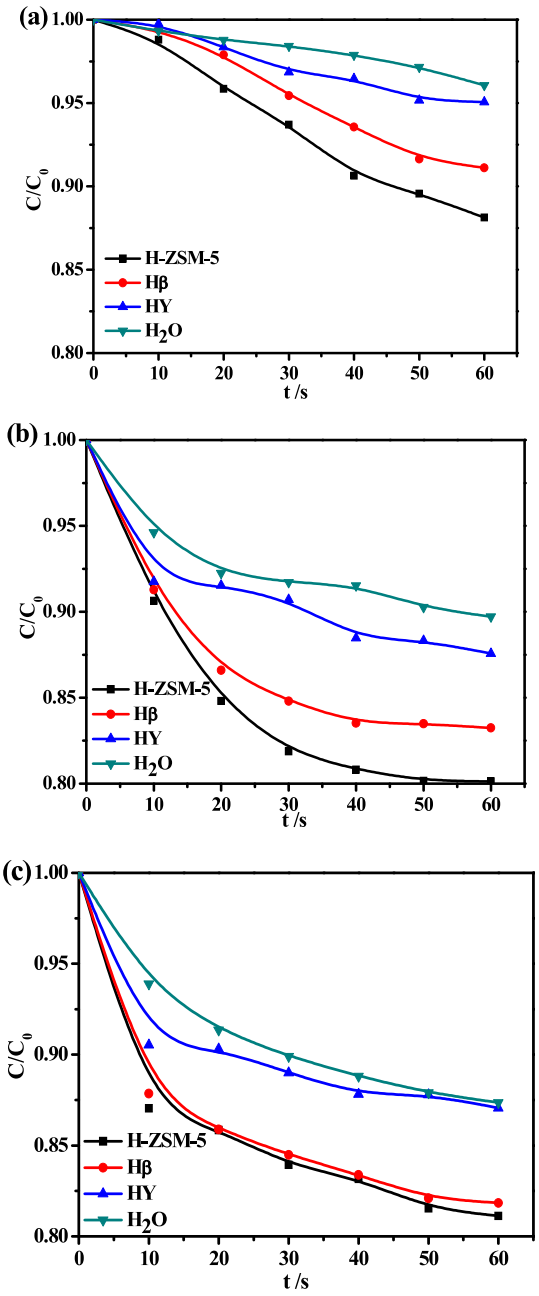

Fig. 6. (a) Effect of catalyst addition (H-ZSM-5) on the average reaction rate with ethylene oxide concentration of 1% (v/v) at 313 K. (b) Arrhenius curve under catalytic and non-catalytic reactions; Other conditions: catalyst addition 10 mg; EO concentration 1% (v/v)

Table 3
3 Calculated values of k for the uncatalyzed and catalyzed hydration reaction at different temperature.

Zeolites	k/(s^{-1} g^{-1})			A/(s^{-1})
	30 °C	40 °C	50 °C	
H-ZSM-5	0.296	0.334	0.439	1.63
Hβ	0.241	0.298	0.428	24.3
HY	0.156	0.256	0.312	124
H_2O	0.151	0.232	0.309	165

Table 4
Calculated reaction rate for the catalyzed hydration reaction at 303 K.

Zeolites	k/(s^{-1} g^{-1})	Initial reaction rate (μmol L^{-1} g^{-1} s^{-1})	Surface area (m^2 g^{-1})	Initial area rate (μmol L^{-1} s^{-1} m^{-2})
H-ZSM-5	0.296	37.0	374	0.0989
Hβ	0.241	25.3	504	0.0502
HY	0.156	18.0	570	0.0316

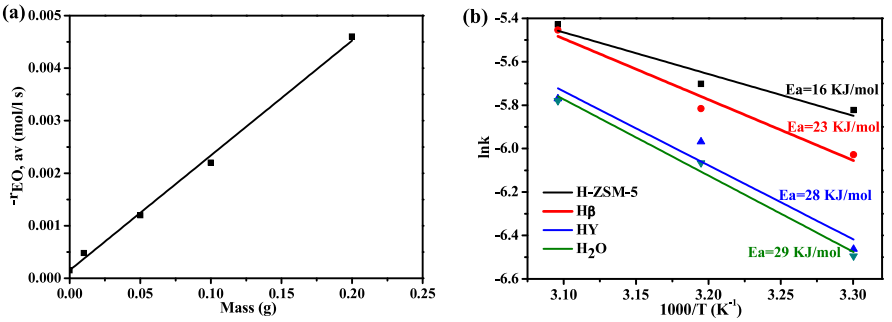

Fig. 7. Time courses of the hydration degradation of EO at (a) 303 K (b) 313 K (c)323 K. Other conditions: catalysts addition 10 mg.

desorbed alcohol diffuses into the solution. The reaction rate is determined by the diffusion, adsorption, desorption, and surface reaction rates of the material. To explore the intrinsic reaction kinetics of the reaction, the effects of diffusion on the reaction must be known. Thus, we conducted research on the relationship between the average reaction rate and the catalyst addition. The experiments were conducted at different H-ZSM-5 additions with EO concentration of 1% (v/v) at 313 K. The catalyst addition varied over a range of 10–200 mg in the reaction mixture. The reaction was allowed to complete 80% EO conversion. Under these conditions, the average reaction rate was calculated by Eqs. (3)–(5). The average reaction rate versus catalyst addition is shown in Fig. 7a. As the figure shows, the average rate linearly increases with catalyst addition, as expected, because the active surface area is proportional to the amount of catalyst. This finding confirms the negligibility of the internal and external diffusion effects (Madon and Boudart, 1982).

3.5.4. Reaction mechanism

Mineral-acid-catalyzed homogeneous EO hydration generally proceeds in the following manner: EO first reacts with acid to form protonated EO, and then the protonated EO reacts with nucleophile H_2O to form a protonated glycol, which transfers a proton to an H_2O molecule to form the glycol and hydronium ion[22]. Although the catalysts studied in the present work are heterogeneous, they are acid catalysts in nature. Thus, the reaction mechanisms should be similar. As a result of the strong polarity of the zeolite surface, water molecules are more easily adsorbed on the surface of zeolite (water permittivity 78.5). Thus, we propose that the reaction first involves the adsorption of H_2O onto acidic sites to form positively charged water species (or Brønsted acidity), leading to the formation of positively charged EO species. Subsequently, the positively charged EO is attacked by nucleophile H_2O, followed by proton transfer to form positively charged MEG. As side reactions, the positively charged absorbed MEG may react with another EO to form diethylene glycol and other high polyalcohols (as shown in Fig. 8).

According to the preceding model description, the hydration reaction of EO was considered to be a series–parallel reaction in four steps. Furthermore, the main reaction can be divided into four steps. The preliminary experimental data show that the formation of a higher level of high polyalcohol is negligible. The reaction equations are listed as follows:

$$EO + H_2O \xrightarrow{\text{Cat.}} MEG \begin{cases} H_20 + * \underset{K_{-1}}{\overset{K_1}{\rightleftarrows}} H_2O* & (1) \\ EO + * \xrightarrow{K_2} EO* & (2) \\ EO* + H_20* \xrightarrow{ks} EG* & (3) \\ EO* \xrightarrow{Kd} EG + * & (4) \end{cases} \tag{3a}$$

$$EO + MEG \xrightarrow{\text{Cat.}} DEG \tag{3b}$$

$$EO + DEG \xrightarrow{Cat.} TEG \tag{3c}$$

$$EO + TEG \xrightarrow{Cat.} PEG. \tag{3d}$$

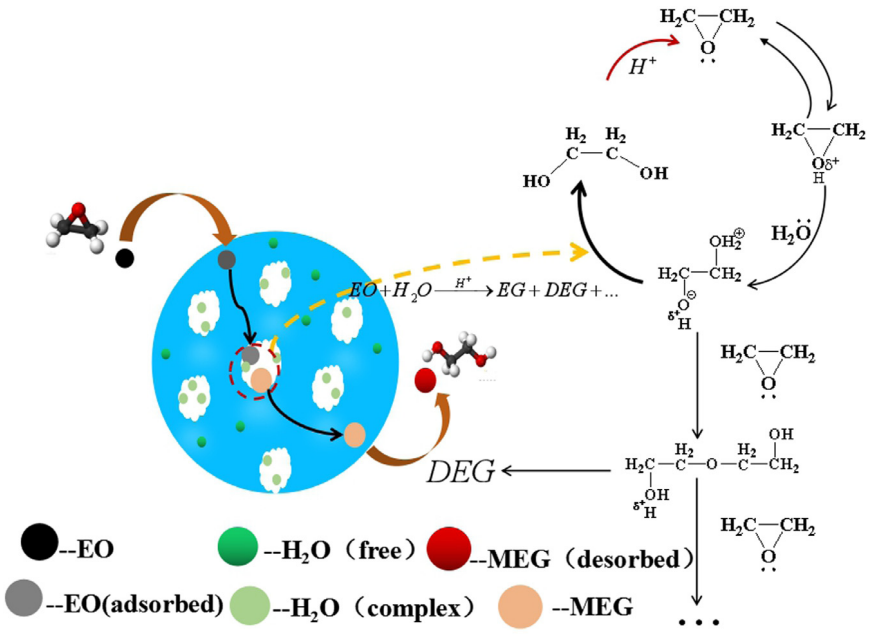

Fig. 8. The model of ethylene oxide catalytic hydration.

4. Conclusion

Zeolites H-ZSM-5, HY, and Hβ are found to be active in EO absorption by solution, and the catalytic activity decreases in the order of H-ZSM-5 > Hβ > HY. H-ZSM-5, which has a high number of Brønsted acid sites, is capable of replacing mineral acids in the acid-catalyzed absorption of EO. Moreover, H-ZSM-5 zeolite with silica–alumina ratio 38 exhibits the best performance due to its high acid density and surface area. In addition, this zeolite remains stable at high concentration and space velocity of 40000 ppm and 24000 mL $h^{-1}g^{-1}$. The kinetic results indicated that the activation energy decreased by 13 kJ/mol. This strategy is expected to lead to the development of a new treatment method for EO exhaust gas.

Acknowledgment

This study was supported by the Natural Science Foundation of China (No. 21506194, No 21676255), the Natural Science Foundation of Zhejiang Province (No. Y16B070011), and the Commission of Science and Technology of Zhejiang province (No. 2017C03007, No. 2017C33106).

References

Al-Jubouri, Sama M., Holmes, Stuart M., 2017. Hierarchically porous zeolite X composites for manganese ion-exchange and solidification: Equilibrium isotherms, kinetic and thermodynamic studies. Chem. Eng. J. (308), 476–491.

Altiokka, Mehmet Riza, Akyalcin, Sema, 2009. Kinetics of hydration of ethylene oxide in the presence of heterogeneous catalyst. Ind. Eng. Chem. Res (48), 10840–10844.

Chen, X.D., Li, X.G., 2018. Interaction between binder and high silica HZSM-5 zeolite for methanol to olefins reactions. Chem. Eng. Sci. (192), 1081–1090.

Chen, X., Zhao, Z.L., Lu, H.F., 2018. A facile route for spraying preparation of Pt/TiO2 monolithic catalysts toward VOCs combustion. Appl. Catal. A 566, 190–199.

Cheng, W.N., 2013. Method for absorbing ethylene oxide by using ethylene carbonate as absorbent. Chem. Ind. Technol. Dev. (10), 31–33.

Conway, R.A., Waggy, G.T., Spiegel, H., Berglund, R.L., 1983. Environmental fate and effects of ethylene oxide. Environ. Sci. Technol. 17, 107.

Corma, A., 1995. Inorganic solid acids and their use in acid-catalyzed hydrocarbon reactions. Cheminform 26 (37), 559–614.

Emeis, C.A., 1993. Determination of integrated molar extinction coefficients for infrared absorption bands of pyridine adsorbed on solid acid catalysts. J. Catal. (141), 347–354.

Ethylene oxide for industry use:GB/T 13098:2006.

Hal, J.W.V., Ledford, J.S., Zhang, X., 2007. Investigation of three types of catalysts for the hydration of ethylene oxide (EO) to monoethylene glycol (MEG). Catal. Today 123 (1–4), 310–315.

Kamal, M.S., Razzak, S.A., Hossain, M.M., 2016. Catalytic oxidation of volatile organic compounds (VOCs) – A review. Atmos. Environ. 140, 117–134.

Lemanski, M.F., Kunin, R., 2000. Catalyst Stabilizing Additive in the Hydrolysis of Alkylene Oxides: US. US 6156942 A.

Li, J., Liu, S., Zhang, H., et al., 2016. Synthesis and characterization of an unusual snowflake-shaped ZSM-5 zeolite with high catalytic performance in the methanol to olefin reaction. Chin. J. Catal. 37 (2), 308–315.

Li, H., Wang, Y., Chen, X., et al., 2018. Preparation of metallic monolithic Pt/FeCrAl fiber catalyst by suspension spraying for VOCs combustion. Rsc Adv. 8 (27), 14806–14811.
Li, Y., Yan, S., Qian, L., et al., 2006. Effect of tin on Nb_2O_5 / α-Al_2O_3, catalyst for ethylene oxide hydration. J. Catal. 241 (1), 173–179.
Li, Y., Yan, S., Yang, W., et al., 2005. Effects of support modification on Nb2O5/a-Al2O3 catalyst for ethylene oxide hydration. J. Mol. Catal. A: Chemical 226 (2), 285–290.
Lu, H.F., Zhou, Y., Han, W.F., et al., 2013. High thermal stability of ceria-based mixed oxide catalysts supported on ZrO_2 for toluene combustion. Catal. Sci. Technol. 3 (6), 1480–1484.
Madon, R.J., Boudart, M., 1982. Experimental criterion for the absence of artifacts in the measurement of rates of heterogeneous catalytic reactions. Ind. Eng. Chem. Fundam. 21, 438.
Maihom, Thana, Namuangruk, Supawadee, et al., 2008. Theoretical study on structure and reaction mechanisms of ethylene oxide hydration over H-ZSM-5: Ethylene Glycol formation. J. Phys. Chem. C (112), 12914–12920.
McKetta, John J., Cunningham, William A., 1984. Encyclopedia of Chemical Processing and Design. 20. CRC Press, p. 309.
Olegario, et al., 2018. Novel ZnO nanostructures on Philippine natural zeolite (PNZ) framework designed via thermal decomposition process of solution-based $ZnCl_2$ precursor. Mater. Res. Express.
Pinto, T.D.J.A., 2006. Sterilization: Ethylene Oxide. Chapter. p. 4370.
Shvets, V.F., Kozlovskiy, R.A., Kozlovskiy, I.A., et al., 2005. The cause and quantitative description of catalyst deactivation in the ethylene oxide hydration process. Chem. Eng. J. 107 (1), 199–204.
Wang, F., Chen, J., Zhang, B., et al., 2005. Hydration of ethylene oxide over modified silica gel. Chin. J. Catal. 26 (5), 355–356.
Yang, D.J., 1982. The theory and application of buffer combustion method for treating organic waste gas. Chongqing Environ. Sci. (5), 25–29.
Yang, Z.J., Li, Y.F., Wu, Q.B., et al., 2011. Layered niobic acid with self-exfoliatable nanosheets and adjustable acidity for catalytic hydration of ethylene oxide. J. Catal..
Yang, X.L., Zhang, Z.C., 2014. One treatment device for ethylene oxide. CN 203507806 U.
Ziolek, M., Nowak, I., Lavalley, J.C., 1997. Acidity study of Nb-containing MCM-41 mesoporous materials. Comparison with that of Al-MCM-41. Catal. Lett. 45 (3–4), 259–265.